

Theoretical mineralogy, density, seismic wavespeeds and H₂O content of the Cascadia subduction zone, with implications for intermediate-depth seismicity and earthquake hazard

Bradley R. Hacker¹, Geoffrey A. Abers² and Simon M. Peacock³

¹ Department of Geological Sciences, University of California, Santa Barbara, California, 93106–9630, USA

² Department of Earth Sciences, Boston University, 675 Commonwealth Avenue, Boston, Massachusetts, 02215, USA

³ Department of Geological Sciences, Arizona State University, Box 871404, Tempe, Arizona, 85287–1404, USA
hacker@geology.ucsb.edu, abers@bu.edu, peacock@asu.edu

ABSTRACT

We calculate physical properties of rocks in subduction zones using a compilation of mineral physical property measurements, a new set of phase diagrams and subduction-zone thermal models, and apply our results to Cascadia. Observed *P*-wave speeds of the Juan de Fuca plate west of the Cascadia trench are best matched by a greenschist-facies upper crust and metastable, partially hydrated lower crust and mantle. The predicted positions of dehydration reactions in the subducting crust show a spatial link to observed seismicity, suggesting that dehydration may be the cause of the earthquakes and that the predicted location of dehydration reactions in the slab can be used to predict hazardous seismicity the length of Cascadia.

Introduction

Much about subduction zones remains unknown because all our information comes either from indirect geophysical observations or observation of fossil subduction zone rocks. In particular, we would like to understand: the hydration state of the mantle wedge and the incoming slab; where and why slabs devolatilize and how this contributes to arc volcanism; slab buoyancy and shape; seismic wavespeeds and their relation to mineralogy; and intermediate-depth earthquakes and their possible relationship to phase transformations. This study uses a synergistic thermal–petrological–seismological approach to address some of these questions. Our approach comprises six specific steps:

- 1) Compile and assess physical properties of minerals relevant to subduction zones.
- 2) Construct phase diagrams apropos to subduction zone rock types and physical conditions.
- 3) Compute pressures (*P*) and temperatures (*T*) for a specific subduction zone.

- 4) Superimpose calculated phase relations onto the *P*–*T* model.
- 5) Superimpose rock physical properties onto the *P*–*T* model.
- 6) Compare predictions to observations.

1. Compiling mineral properties

We performed an extensive literature search to obtain physical properties of minerals relevant to subduction zones. The necessary physical properties are: formula weight, molar volume, H₂O content, expansivity α , $\partial\alpha/\partial T$, the isothermal bulk modulus K_T , $\partial K_T/\partial P$, the shear modulus μ , $\partial\mu/\partial T$, $\partial\mu/\partial P$, the Grüneisen parameter γ_{th} and the second Grüneisen parameter δ_T . From these we used a second-order finite-strain approximation (which yields negligible error at these pressures for which $P/K_T < 1$) to calculate the adiabatic bulk modulus, shear modulus, density, seismic wavespeeds and Poisson's ratios for each mineral as a function of *P* and *T*. Each of these values was examined in some detail to ensure that the calculated values were in agreement with values measured directly on minerals or single-phase mineral aggregates at elevated *P* and *T*.

2. Constructing phase diagrams

We chose to simplify the rock compositions under consideration to basalt/gabbro, lherzolite, harzburgite and serpentinite—i.e., the entire overriding plate crust and subducting plate crust was treated as basalt/gabbro, and the remainder was considered ultramafic. We then calculated the *P*–*T* stability fields of different minerals and the reactions that bound the various fields. These phase diagrams permit direct assessment of phase proportions, reaction stoichiometries, H₂O content, and, in combination with the rock physical property calculations described above, density, V_p and V_s of mafic and ultramafic rocks in subduction zones.

To create a phase diagram for mafic rocks, we performed an extensive literature search to identify studies that reported all three of the following: 1) bulk rock compositions; 2) mineral modes; and 3) mineral compositions. From these studies we chose only rocks whose bulk compositions differed from mid-ocean ridge basalts (MORB) by less than $\sim 10\%$. Assuming that the entire crust is of MORB composition is clearly incorrect for the lower crust, as detailed below. We then compiled the mineral modes and mineral compositions into various metamorphic facies. Next, the P - T range over which each mineral assemblage is stable was defined using Thermocalc [Holland and Powell, 1998]. Most boundaries are thus defined by discontinuous reactions involving the appearance or disappearance of at least one phase. Obvious outliers were discarded, and a mean mineral mode and set of mineral compositions was computed for each metamorphic facies.

Phase diagrams for lherzolite, harzburgite and serpentinite were constructed principally from Thermocalc [Holland and Powell, 1998] using Mg-endmember reactions in the Ca-Fe²⁺-Mg-Al-Si-H-O system and mineral compositions reported in the literature for naturally metamorphosed ultramafic rocks. Thermocalc's calculations of phase relations at $P > 5$ GPa were modified in light of recent experiments by Luth [1995], Ulmer and Trommsdorff [1995], Wunder and Schreyer [1997], Bose and Navrotsky [1998], Wunder [1998] and Pawley [2000].

3. Computing subduction-zone pressure and temperature

For Cascadia, we used the thermal model of Wang *et al.* [1995] calculated for southern Vancouver Island (Figure 1a). Pressures for the same cross section were calculated using appropriate rock densities.

4. Superimposing phase relations

Onto a subduction-zone cross section depicting P and T and rock composition, we overlaid the different metamorphic mineral assemblages computed in step 2. Figures 1b and 1c show the results for mafic rocks and harzburgite, respectively. We have assumed that the activity of $H_2O = 1$ (or that $P_{H_2O} = P_{lithostatic}$) and that equilibrium obtains. These assumptions cannot be correct everywhere and are addressed partially in a later section.

5. Superimposing rock physical properties

From the mineral physical properties calculated at elevated P and T in step 1, we derived rock physical properties using a Voigt-Reuss-Hill average weighted by mineral proportions determined in step 2. The results are shown in Figures 1d-1g.

6. Comparing predictions to observations: Cascadia

Beneath Cascadia, the 5-9 Ma Juan de Fuca plate

subducts at a rate of 41 mm/yr [Hyndman and Wang, 1993], rendering it among the youngest, most slowly subducting, and, consequently, warmest slabs in the world. The slab has a thick sediment blanket and upper plate volcanism is weak to moderate.

Seismicity: the correlation to dehydration

In the vicinity of southern Vancouver Island, seismicity along and near the intraplate subduction thrust occurs in two distinct pulses—one at 30-40 km depth and another around 70 km depth [Rogers *et al.*, 1990] (Figure 1a). It is a primary observation of this study that there is a spatial correlation between this seismicity and the predicted dehydration reactions in the subducting crust (Figure 1b). The upper nest of earthquakes at 30-40 km depth falls within the lower half of the epidote amphibolite field and stops abruptly at the down dip end at the transition to zoisite-amphibole eclogite. This corresponds to a predicted change from 2.1 to 0.7 wt. % crystallographically bound H_2O . The lower nest of earthquakes at ~ 70 km depth coincides with the transition from zoisite-amphibole eclogite to anhydrous eclogite—a reduction in H_2O content from 0.3 to 0.1 wt. %. In other words, along the south Vancouver Island transect, the bulk of the seismicity occurs at depths coincident with predicted dehydration in the downgoing crust. This same spatial correlation between phase transformations in the crust and intermediate-depth seismicity holds for the Nankai (southern Japan) and Tohoku (northern Japan) subduction zones where thermal conditions are different. We propose, therefore, that calculating the position of dehydration reactions in the slab could be an inexpensive and effective means of predicting future hazardous seismicity; certainly this hypothesis can easily be tested with additional modeling.

The idea that intermediate-depth slab seismicity might be related to dehydration reactions in the upper part of the slab was explored in considerable detail by Kirby *et al.* [1996], Peacock and Wang [1999] and Kirby [2000]. Our calculations for Cascadia provide a very strong confirmation of this hypothesis. Moreover, the fact that the seismicity correlates well with phase changes predicted from equilibrium considerations implies that at least part of the subducted crust is undergoing mineralogical change in a near-equilibrium fashion. Abundant geologic evidence from localities around the globe demonstrates that fine-grained, H_2O -rich basalts transform to high-pressure mineralogies faster than coarse-grained, H_2O -poor gabbros [Hacker, 1996]. Thus, in a subducting slab, we expect phase transformations in the gabbroic layer to lag those in the volcanic layer and produce dehydration at greater depths than predicted by equilibrium considerations. Therefore it is likely that: 1) the observed seismicity is generated principally by dehydration reactions in the volcanic layer of the subducted crust, which trans-

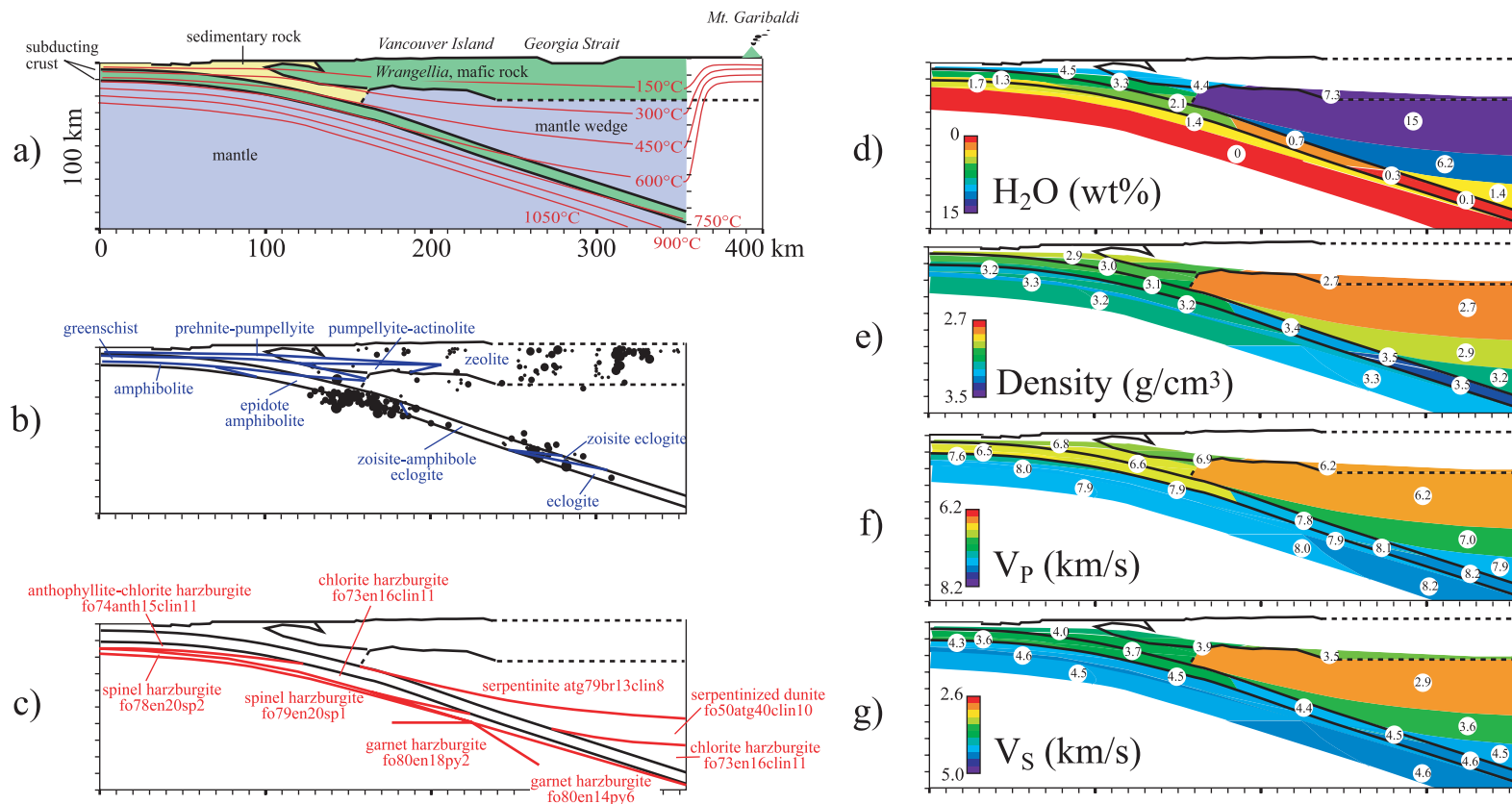


FIGURE 1: Calculated properties of the Cascadia subduction zone along a transect through southern Vancouver Island. a) Geology [Hyndman and Wang, 1993] and isotherms [Wang et al., 1995]. b) Calculated phase relations in mafic crust and observed seismicity [Rogers et al., 1990]. c) Calculated phase relations in ultramafic rock. Numbers indicate volume of minerals by percentage: anth, anthophyllite (amphibole); atg, antigorite (serpentine); br, brucite; clin, clinoclchlore (chlorite); en, enstatite (orthopyroxene); fo, forsterite (olivine); sp, spinel; py, pyrope (garnet). d) Calculated H₂O content. e) Calculated densities. f) Calculated P-wavespeeds. g) Calculated S-wavespeeds.

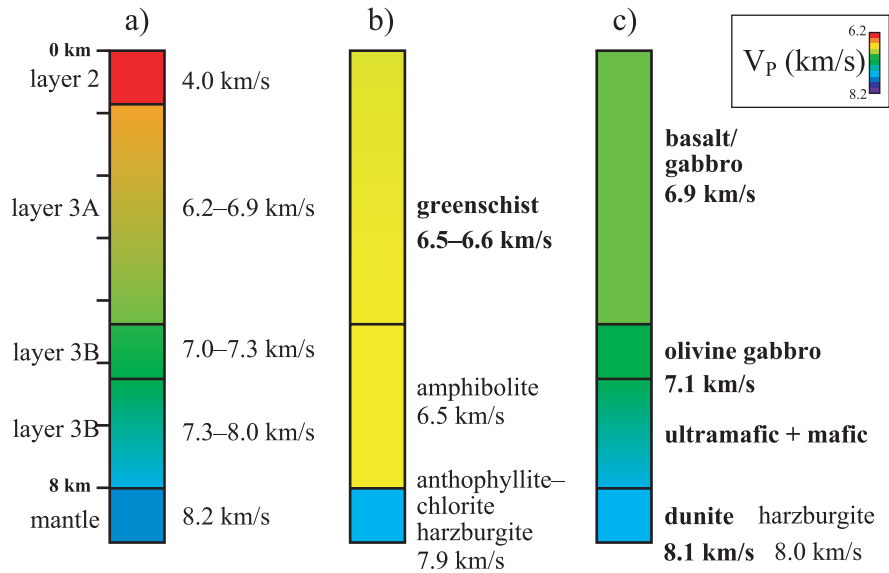


FIGURE 2: Observed and calculated P -wavespeeds for the Juan de Fuca plate offshore Vancouver Island. a) Seismic section from Clowes [2000]. b) P -wavespeeds calculated assuming $a_{\text{H}_2\text{O}} = 1$. c) P -wavespeeds calculated assuming $a_{\text{H}_2\text{O}} = 0$. Calculations in b) and c) are based on pressures and temperatures from most-outboard portion of Hyndman and Wang's [1993] thermal model. Best fits to seismic observations are indicated with boldface type.

forms on a near-equilibrium basis to eclogite; and 2) the subducted plutonic layer is nearly anhydrous, generates few earthquakes and transforms to eclogite at greater depth than predicted by equilibrium considerations.

Slab velocities and mineralogy

An ocean-bottom seismometer survey offshore and parallel to Vancouver Island by Clowes [this volume] can be compared with our predicted wavespeeds for the Juan de Fuca plate. Clowes' interpretation (Figure 2a) is that the Juan de Fuca plate includes: a one kilometer thick layer 2 with $V_p = 4.0$ km/s; a four kilometer thick layer 3A with $V_p = 6.2\text{--}6.9$ km/s; a layer 3B split into a one kilometer layer with $V_p = 7.0\text{--}7.3$ km/s above a two kilometer layer with $V_p = 7.3\text{--}8.0$ km/s; and an underlying mantle with a P -wave speed of 8.2 km/s.

In our equilibrium model (Figure 2b), layers 2 and 3A have a greenschist-facies mineralogy and a P -wave speed of 6.6 km/s. Layer 3B is at amphibolite facies and has $V_p = 6.5$ km/s. The immediately underlying mantle is predicted to be an anthophyllite–chlorite-bearing harzburgite with a P -wave speed of 7.6 km/s.

Thus, we do not successfully model layer 2, but this may be because we do not consider the effects of porosity and fluids. At greater pressures where fluids are expelled and pores closed, our model may be correct. The faster-than-predicted speeds (>6.6 km/s) in the base of layer 3A imply that the lower part of that layer is not at greenschist facies. Studies of ophiolites imply that the most likely candidate is unaltered basalt/gabbro. If we model

layers 3A and 3B as unaltered, metastable basalt/gabbro of MORB composition, we calculate a speed of 6.9 km/s (Figure 1c). Speeds of 7.0–7.3 km/s in the upper one kilometer of layer 3B are also faster than in our model, implying that layer 3B is not amphibolite-facies gabbro. Moreover, the observed speeds are faster than our calculated speeds for metastable gabbro of MORB composition. Such speeds are, however, compatible with calculated speeds for pyroxene gabbro or olivine gabbro. Speeds of 7.3–7.8 km/s in the lower one kilometer of layer 3B can be modeled as a mix of olivine gabbro, wehrlite and clinopyroxenite. Our calculated speed for anthophyllite–chlorite-bearing harzburgite is slow compared to the observed seismic wave speed and the reported V_p implies a mix of anhydrous harzburgite and dunite.

Trying to match the measured seismic P -wavespeeds with specific homogeneous rock types is fraught with uncertainty. However, the best match is attained assuming that: 1) layer 3A is greenschist facies at the top and grades downward into an anhydrous, metastable basalt; 2) layer 3B is not MORB-composition gabbro; and 3) the mantle is metastable, anhydrous harzburgite. Alternatively, the velocity gradient observed by Clowes [this volume] at the bottom of the crust may reflect lateral and/or vertical resolution limits of the seismic data and a more complex crust-mantle boundary than assumed.

Conclusions

Our model produces calculated physical properties of rocks in subduction zones using a compilation of mineral

physical property measurements, a new set of phase diagrams and subduction-zone thermal models. Comparison of predicted vs. observed P -wavespeeds indicates that the lowermost crust and mantle of the Juan de Fuca plate west of the Cascadia trench is not at mineralogical equilibrium with the ambient P and T and, specifically, is not fully hydrated. A distinctive correlation between the predicted positions of dehydration reactions in the subducting crust and observed seismicity suggests a causal link between the two and that future hazardous seismicity the length of Cascadia can be predicted via our method.

Acknowledgements

Thanks to Steve Kirby and Kelin Wang and their respective institutions for hosting the Victoria Workshop. Steve was also the first to suggest the use of mapping dehydration reactions in the slab as an indicator of future seismicity.

References

- Bose, K., and A. Navrotsky, Thermochemistry and phase equilibria of hydrous phases in the system $\text{MgO-SiO}_2\text{-H}_2\text{O}$; implications for volatile transport to the mantle, *J. Geophys. Res.*, *103*, 9713–9719, 1998.
- Clowes, R.M., Crustal structure of northern Juan de Fuca plate and Cascadia subduction zone—new results, old data, in *The Cascadia Subduction Zone and Related Subduction Systems*, edited by S.H. Kirby, K. Wang, and S.G. Dunlop, pp. 55–58, U.S. Geological Survey Open-File Report 02–328, Geological Survey of Canada Open File 4350, 2002.
- Hacker, B.R., Eclogite formation and the rheology, buoyancy, seismicity and H_2O content of oceanic crust, in *Dynamics of Subduction*, edited by G.E. Bebout, D. Scholl, S.H. Kirby, and J.P. Platt, pp. 337–246, American Geophysical Union, Washington, D.C., 1996.
- Holland, T.J.B., and R. Powell, An internally consistent thermodynamic data set for phases of petrological interest, *J. Metamorph. Geol.*, *16*, 309–343, 1998.
- Hyndman, R.D., and K. Wang, Thermal constraints on the zone of possible major thrust earthquake failure on the Cascadia margin, *J. Geophys. Res.*, *98*, 2039–2060, 1993.
- Kirby, S.H., Taking the temperature of slabs, *Nature*, *403*, 31–33, 2000.
- Kirby, S.H., E.R. Engdahl, and R. Denlinger, Intermediate-depth intraslab earthquakes and arc volcanism as physical expressions of crustal and uppermost mantle metamorphism in subducting slabs, in *Subduction Top to Bottom, Geophysical Monograph*, edited by G.E. Bebout, D. Scholl, and S. Kirby, pp. 195–214, American Geophysical Union, Washington, D.C., 1996.
- Luth, R.W., Is phase A relevant to the Earth's mantle?, *Geochimica et Cosmochimica Acta*, *59*, 679–682, 1995.
- Pawley, A., Stability of clinohumite in the system $\text{MgO-SiO}_2\text{-H}_2\text{O}$, *Contributions to Mineralogy and Petrology*, *138*, 284–291, 2000.
- Peacock, S.M., and K. Wang, Seismic consequences of warm versus cool subduction metamorphism: examples from southwest and northeast Japan, *Science*, *286*, 937–939, 1999.
- Rogers, G.C., C. Spindler, R.D. Hyndman, and J.L. Vasek, Seismicity along the Vancouver Island Lithoprobe corridor, *Lithoprobe Report*, *11*, 166–169, 1990.
- Ulmer, P., and V. Trommsdorff, Serpentine stability related to mantle depths and subduction-related magmatism, *Science*, *268*, 858–861, 1995.
- Wang, K., T. Mulder, G.C. Rogers, and R.D. Hyndman, Case for very low coupling stress on the Cascadia subduction fault, *J. Geophys. Res.*, *100*, 12,907–12,918, 1995.
- Wunder, B., Equilibrium experiments in the system $\text{MgO-SiO}_2\text{-H}_2\text{O}$ (MSH); stability fields of clinohumite-OH [$\text{Mg}_9\text{Si}_4\text{O}_{16}(\text{OH})_2$], chondrodite-OH [$\text{Mg}_5\text{Si}_2\text{O}_8(\text{OH})_2$] and phase A ($\text{Mg}_7\text{Si}_2\text{O}_8(\text{OH})_6$), *Contributions to Mineralogy and Petrology*, *132*, 111–20, 1998.
- Wunder, B., and W. Schreyer, Antigorite: high-pressure stability in the system $\text{MgO-SiO}_2\text{-H}_2\text{O}$ (MSH), *Lithos*, *41*, 213–227, 1997.